Available online at www.sciencedirect.com

SciVerse ScienceDirect

Physics Procedia 42 (2013) 31 – 38

Physics Procedia

PNCMI 2012 - Polarized Neutrons for Condensed Matter Investigations 2012

Imaging Quantum Mechanical Effects in Superconductors with Polarized Neutrons

W. Treimer[1,a,b], O. Ebrahimi[b] and N. Karakas[a,b]

[a] *University of Applied Sciences, FB II, Luxemburgerstr. 10, D - 13353 Berlin, Germany*

[b] *Helmholtz Center Berlin Wannsee, Joint Department G-G1, Hahn-Meitner-Platz 1, D - 14109 Berlin, Germany*

Abstract

Macroscopic Quantum effects such as the Meissner effect and magnetic flux trapping in massive, pure poly-crystalline lead samples and in a low purity crystalline sample having non-superconducting parts could be visualized and quantified by radiography with polarized neutrons. A uniform poly-crystalline Pb sample with a high purity of $1-1\times10^{-4}$ weight% and one with a low purity of approx. 85 weight% Pb having non-superconducting parts showed a partial Meissner effect and for $B_{ext} = 0$ and $T < T_c$ a non-uniform magnetic flux trapping. Based on radiographies with polarized neutrons the trapped and expelled magnetic fields could be calculated for the uniform lead sample, in the case of the sample which contains non-superconducting parts an asymmetric (also squeezed) field distribution yielded the best fit .

Keywords: Polarized neutrons, neutron imaging, superconductivity, Meissner effect, flux pinning, lead
PACS: 74.20.-z, 74.25.Ha, 74.70.-b,28.20.Pr,

[1] Email: treimer@helmholtz-berlin.de

doi:10.1016/j.phpro.2013.03.172

1. Introduction

The investigations of the Meissner effect (complete expulsion of an external magnetic field in the superconducting state) and flux pinning in superconductors type I and type II are one of the most exciting macroscopic quantum effects that were investigated since the discovery of superconductivity by Kammerling Onnes in 1911. A weak external magnetic field applied on a sample is expelled if the sample is cooled down below a critical temperature T_c. The sample behaves like a perfect diamagnetic material. What is less known is the effect of flux trapping or flux pinning in type I superconductors. This effect occurs if in the Meissner state the external magnetic field is switched off and a part of it remains "trapped" or "pinned" in the sample. This is observed usually in type-II superconductors and attributed to grain boundaries and cracks in a crystalline sample. However, already in the late 1930ties Landau pointed out that flux pinning also happens in type-I superconductors and he published a model to explain the surface structures which were observed at several samples [1]. A large number of publications dealing with the Meissner effect and flux pinning tried to explain the different (surface) observations, but no generally accepted theory could describe all the experimental results sufficiently well. [2] - [13]. The main cause may be found in that all experiments were surface observations and the samples usually had rather two-dimensional than three-dimensional shape i.e. they were discs. Despite high resolution magneto-optical imaging all conclusions concerning fields in the bulk of samples remain "surface-deduced-phenomena" [15] - [17].

Recent experiments with type-I superconductors and polarized neutrons allowed for the first time a detailed look inside samples when they are in the Meissner and in the intermediate state (intermediate state: T < T_c, external magnetic field is off) [18], [19]. In highly pure and homogeneous lead the commonly expected Meissner effect and an homogeneously distributed flux pinning in samples could *not* be observed but partially and total suppressed Meissner effect as well as squeezed flux trapping as was also observed in type-II superconducting Nb [20]. Here we present new results of these phenomena.

2. Theory

In order to observe the Meissner effect and flux pinning in the bulk of samples by imaging methods one has to use a radiation which once weakly interact with materials, i.e. exhibit low attenuation when it traverses the sample and which is "sensitive" to magnetic fields. Both criteria are fulfilled by polarized neutrons. In order to probe a magnetic field inside or outside of a sample the interaction of the spin with the field must be considered in detail. The neutron spin in a magnetic field behaves like a small magnet which motion is described by

$$\frac{dS(t)}{dt}_j = \frac{\mu_N}{h} g\left[\vec{S}(t) \times \overrightarrow{B}(t)\right]_j \quad j = x, y, z \tag{1}$$

with the nuclear magneton $\mu_N = 5.05078343 \cdot 10^{-27}$ [J/T] and the Land-factor for neutrons g = −3.826085, h = $6.6260755 \cdot 10^{-34}$ [J.s], $\hbar$ = h/2π . For thermal and cold neutrons the spin can be described like a classical magnetic moment having the Larmor frequency $\omega_L = \gamma_L \cdot B$ with γ_L = gyromagnetic ratio of the neutron, γ_L = g · μ_N /$\hbar$ = -1.83247x10^8 [rad·s^{-1} · T^{-1}]. With the Larmor frequency ω_L the total angle of rotation ϕ becomes after the passage through a magnetic field B after a time t as

$$\phi = \omega_L \cdot t = \gamma_L \cdot B \cdot t = \frac{\gamma_L}{v} \int B \cdot ds = \frac{\gamma_L \cdot m}{h} B \cdot s \cdot \lambda \tag{2}$$

v = velocity of the neutron, B = magnetic field, m = neutron mass, s path length in the field, λ = wavelength. The path integral $\int B \cdot ds$ and the wavelength λ determine ϕ and thus the final depolarization of the initially fully polarized neutron beam. A neutron beam that traverses a sample will experience a two-dimensional path-dependent depolarization which must be two-dimensionally analyzed and registered. For this purpose one has to know (calculate) the path integrals and with them the spin rotation angles ϕ. A very elegant way to calculate the path integrals is to use a projection of the Radon Transform R{f} [21] that can be applied to

magnetic fields as well:

$$
\begin{aligned}
R_{0,\alpha=const}\{f\} = \hat{f}_0(p,\alpha) &= \int_{-\infty}^{\infty}\int_{-\infty}^{\infty} B(x,z)\cdot\delta(p - x\cdot\cos(\alpha) - z\cdot\sin(\alpha))\cdot dx\cdot dz \\
R_{90,\alpha=const}\{f\} = \hat{f}_{90}(p,\alpha) &= \int_{-\infty}^{\infty}\int_{-\infty}^{\infty} B(y,z)\cdot\delta(p - y\cdot\cos(\alpha) - z\cdot\sin(\alpha))\cdot dy\cdot dz
\end{aligned}
\tag{3}
$$

Both Radon transforms R (equations (3)) yield the path integrals for the particular orientation of the sample

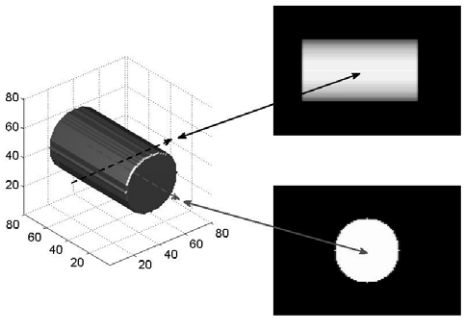

Fig. 1. Two projections of a cylindrical sample, orientation parallel (0°) and perpendicular (90°) to the neutron beam

with respect to the neutron beam. Thus with equ.3 and path length s = R{f} one can calculate ϕ. The result of such a 2D radiography (with or without an external magnetic field) is a two-dimensional depolarization matrix which is used to determine the amount and the shape of the expelled and trapped/pinned magnetic field. For both sample orientations the measured intensities become

$$
\begin{aligned}
I(x,z) &= \underbrace{I_0\cdot T\cdot\exp(-\int_{path}\Sigma(s)ds)}_{I_{att}(x,z)}\cdot\underbrace{\frac{1}{2}(1+\cos\phi(x,z))}_{I_{spin}(x,z)} \\
I(y,z) &= \underbrace{I_0\cdot T\cdot\exp(-\int_{path}\Sigma(s)ds)}_{I_{att}(y,z)}\cdot\underbrace{\frac{1}{2}(1+\cos\phi(y,z))}_{I_{spin}(y,z)}
\end{aligned}
\tag{4}
$$

In order to get a good approximation of the expelled and trapped fields, several 3D models of magnetic fields were assumed, adapted to the sample and the particular Radon transform calculated. Using equations (2) - (4) for both sample orientations parallel and perpendicular to neutron flight direction one could calculate the two-dimensional image due to the spin-depolarization if the neutron passes through a magnetic field. The sensitivity of this method is good, keeping in mind that for B = 10mT and a neutron wavelength λ=0.4nm a path length s = 1.7mm flips the spin from up to down.

The boundary condition for these calculations was that B must become small at the edges of the sample, because no depolarization was observed there. The next assumption was, that B_{trapp} (trapped field) must be smaller than B_{ext} (external applied field) and the sum of B_{expel} (expelled field) and B_{trapp} must not exceed B_{ext}. In all cases the sample under investigation was 3D-modelled and different magnetic fields "added" to the sample (cp. Fig.1 and Fig.5). Several previously performed experiments with other lead samples suggested a non-uniform distribution of the trapped field, which was verified before. Thus the resulting two-dimensional depolarization patterns had to be modelled in such a way that the calculated images come close to the experimental results. Assuming a trapped field as shown in Fig.2 one could fit very well the calculated data to the experimental ones (see below).

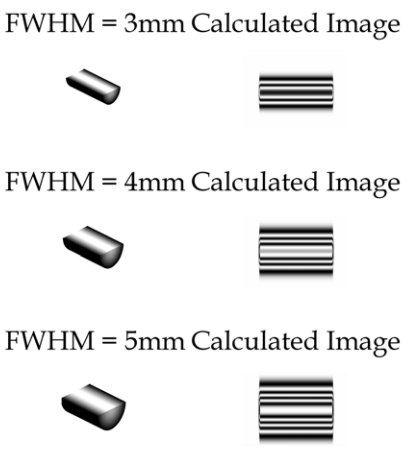

Fig. 2. Left part: Shape of the trapped magnetic field using the Radon transform of different B-fields. Right part: Calculated image using polarized neutrons. Note the sensitivity of the FWHM of the Gaussian shaped field on the fringe pattern and its extent. The sample was a lead cylinder, 12mm diameter and 30mm length

3. Experimental results

All experiments were performed with the new instrument for polarized neutron tomography "PONTO" (*Po*larized *N*eutron *To*mography, see Fig.3) at the BER II reactor (Berlin) [18]. A graphite monochromator (C [002] - reflection) reflected a mean wave length of 0.39 (1)nm to the optical bench which was equipped with an horizontal (0.2°) and a vertical (0.1°) collimator, a solid state polarizer, sample goniometer, (and translation slides), a spin-analyzer and a 2D - detector. The overall polarization was measured as 85(5)%. The samples under investigations were kept in special sample holders in the cryostat and cooled down from room temperature first to 8K > T_c(Pb) = 7.19K and then in several steps down to 5.5K. We investigated the

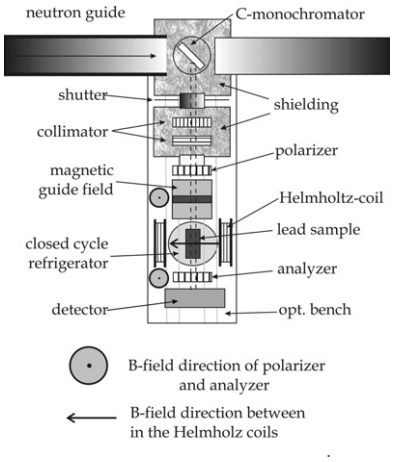

Fig. 3. Instrument "PONTO" for imaging with polarized neutrons

Meissner state and flux pinning in several samples of lead (type-I superconductor) testing the capabilities of PONTO. The cylindrical lead samples had all a diameter of 12mm and a length of 30mm. The purity of these samples were given as $1 - 10^{-4}$weight-%. In a previously performed series with a lead single crystal the complete expulsion of the external magnetic field could be measured if the sample was kept at

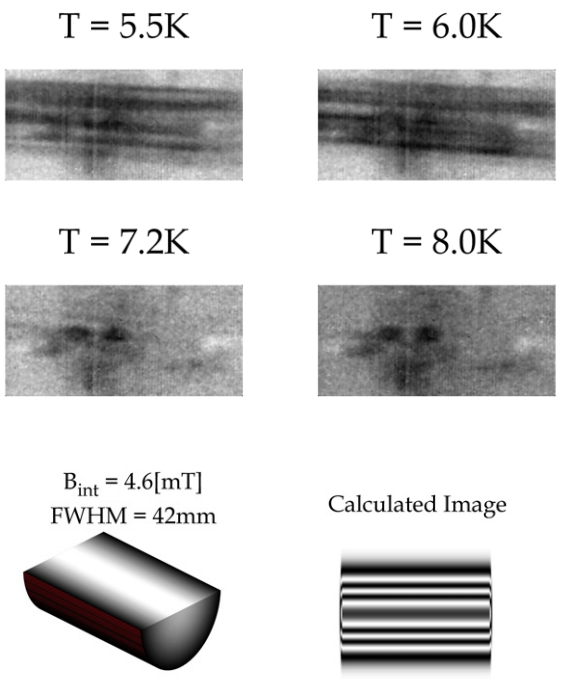

Fig. 4. Trapped magnetic fields at T = 5.5K and T = 6.K, fringes disappear for T > T_c = 7.19: no pattern for T = 7.2K and T = 8.0K, B_{ext} = off, bottom : calculation of the B - field and its image. Best fit for $B_{trapp} = B_{int}$ = 4.6mT

T < T_c = 7.19K, consequently no flux trapping could be observed [19]. Investigating the poly-crystalline sample which had a measured purity of $1 - 10^{-4}$ weight-% the Meissner effect occurred only partially, i.e. a part of the magnetic field was expelled out of and the remaining field was trapped in the sample. Fig.4 shows the results. As can be seen, the fringe pattern disappears if the sample temperature is raised above T_c = 7.19K. Remarkable is the kind of flux trapping. Despite the fact that in the Meissner phase a homogeneous magnetic field was applied to the sample, the field trapping in the intermediate state (B_{ext} is off) was inhomogeneously distributed: Calculations show that in this phase the field is squeezed around the rod axis, parallel to the axis, but perpendicular to the rod axis Gaussian shaped. A comparison with different samples confirmed this behavior. Therefore the calculation of the expelled magnetic field (in the Meissner phase) as well as the trapped field in the case of the intermediate state could be realized for the pure poly-crystalline lead samples [19]. The best fit for the expelled field B_{expel} was 1.6mT, the one for the trapped field B_{trapp} was 4.6mT, the sum below B_{ext} = 6.4mT.

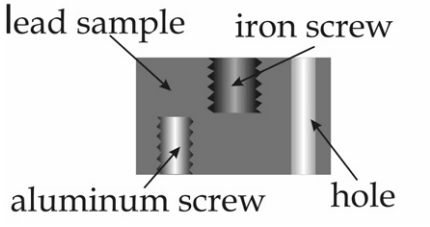

Fig. 5. Poly-crystalline lead sample (cylinder, diameter = 12mm, length = 20mm with inserts: iron diameter = 5mm, aluminum diameter = 3.3mm, hole diameter = 2mm

We also tested ordinary radiation shielding lead concerning the Meissner effect and flux pinning. With this sample the influence of non-superconducting parts on the Meissner phase and on the intermediate phase

of lead was studied (see also [22]). The ordinary lead sample (the components of the shielding lead are given in Table 1) got two different screws and a hole drilled, iron (V2A steel) with a diameter 5mm and aluminum with a diameter 3.3mm and an hole with diameter 2mm. Two Helmholtz coils (diameter 200mm) produced an homogeneous field of 6.4mT on the position of the sample. For each image when the sample was cooled down one had to wait for approx. three hours to guarantee the overall same sample temperature. The exposure time was as well three hours.

Table 1. Elements in Pb shielding sample

Element	weigth - %
C	4.51 - 9.63
O	7.42 - 7.89
Sb	2.18 - 3.32
Al	0.03
Cl	0.03
Sr	0.24
Pb	85.9 - 78.95

For the investigations of the Meissner state the external magnetic field B_{ext} = 6.4mT was applied to the sample during the total cooling process, i.e. from room temperature to 8K and then step-wise down to 5.5K. Images were recorded at T = 8K and 5.5K, at T = 5.5K images once with spin up and then spin down were recorded to identify uniquely the magnetic field expulsion, Fig.6 shows the results.

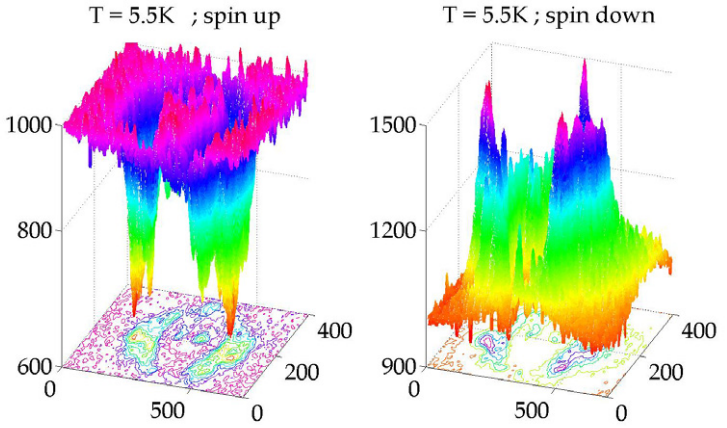

Fig. 6. Meissner effect for spin up and spin down, (x,y) - plane shows the projection, z - axis shows the expelled magnetic field, once measured with neutron spin up and then for neutron spin down

The series was repeated to observe possible flux trapping/pinning in the sample. Again images at T = 8K and T = 5.5K for the sample orientation parallel and perpendicular to the neutron flight direction were measured. For the observations of magnetic flux trapping B_{ext} was switched off, keeping the sample temperature below T_c. As can be seen from Fig.7 at T = 5.5K the iron screw is visible (due to absorption, as well as for T = 8K), the aluminum screw and the hole remain invisible but a fringe pattern arise as was observed for the pure poly-crystalline sample. This fringe pattern in the upper half of the sample appears quite parallel, whereas in the lower half a coarser fringe patterns also outside the sample could be observed. Increasing the sample temperature above T_c(Pb), all patterns disappear, a unique feature of superconductivity.

Fig.8 shows the calculated trapped field of this lead sample in the intermediate state and the corresponding image as it was measured with PONTO. The calculation of the trapped field were performed with the

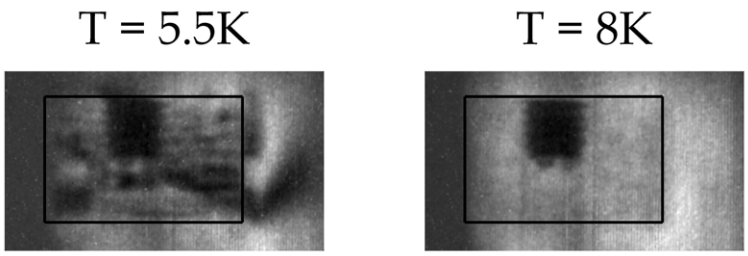

Fig. 7. Lead sample with iron screw; dark area in the upper half, aluminum screw and the hole are invisible. The presence of non-superconducting parts disturb the trapped flux, seen as either non-symmetric parallel fringe pattern or as streaks inside and outside of the sample that vanish completely for T = 8K > T_c.

equations (2) - (4) assuming a similar trapped field as it was used for the poly-crystalline sample. The upper half of the sample could be fitted with B_{trapp} = 1.45mT quite well to the experimental image as can be seen from Fig.8, the lower part, however, could be simulated only qualitatively. The fitting parameter were only the amount of the trapped field and the FWHM of the 3D-Gaussian function (2D-Gaussian in the plane perpendicular to the rod axis, constant parallel to the rod axis).

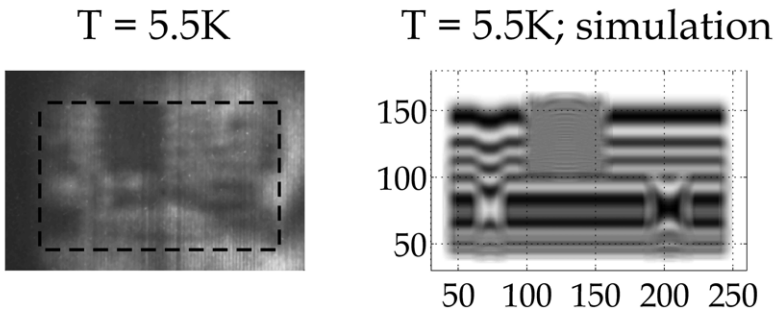

Fig. 8. Measurement and simulation of the trapped field in the composed lead sample in the intermediate state; best fit for the trapped field B_{trapp} = 1.45mT

4. Summary

Polarized neutrons were used to visualize magnetic field expulsion in the Meissner phase and magnetic flux trapping in the intermediate phase of pure poly-crystalline and ordinary superconducting lead samples. In the case of the pure poly-crystalline sample the expelled and trapped magnetic flux could be determined from the neutron images. The sample consisting of ordinary lead got two components, an Fe and an Al screw and a hole, all normal conducting for $5.5K \leq T \leq T_c = 7.2K$, showed a similar behavior in the intermediate state as it was observed in uniform samples, i.e. squeezing the trapped flux, but occurring more complicated and not uniform. The non-superconducting parts apparently influenced both the Meissner effect and flux trapping/pinning, i.e. both effects cannot be considered as isolated effects in the superconducting lead body containing non-superconducting parts.

Acknowledgements

We thank Prof. Dr. Ralf Martens-Menzel (University of Applied Sciences,Beuthhochschule Berlin, Department II) and and Dr. Nelia Wanderka (Helmholtz Zentrum fuer Materialien und Energie Berlin) for their

detailed analysis of the lead samples.
This work was supported by the Federal Ministry of Education and Research (BMBF) project No 05K10KF1 and by the Helmholtz Zentrum fuer Materialien und Energie Berlin Wannsee.

References

[1] L. Landau, Nature **141**, 688 (1938).
[2] A. G. Meshkovsky and A. I. Shalnikov , J. exp. theor. Phys. U.S.S.R., 17, 851 (1947).
[3] J. A. Osborn, Phys. Rev. **67**, 351-357 (1945).
[4] N. V. Sarma and J.R. Moon, Phys. Lett. **24A** , 11, 580 (1967).
[5] A.T. Dorsey and R.E. Goldstein, Phys. Rev. B **57**, 5, 3058-3072 (1998).
[6] R. P. Huebener, Magnetic Flux Structures of Superconductors. 2nd edn, (Springer-Verlag, 2001).
[7] A. Fortini, E. Paumier, Phys. Rev. B, **14**, 1, 55 (1976).
[8] D. J. E. Callaway, Nucl. Phys. B **344**, 627 - 645 (1990).
[9] H. Castro, B. Dutoit, A. Jacquier, M. Baharami, L. Rinderer, L., Phys. Rev. B, **59**, 596 (1999).
[10] M. J. Van Bael,et al., Phys. Rev. B **68**, 014509 (2003).
[11] S.V*é*lez, C. Panades-Guinart, G. Abril, A. Garcia-Santiago, J. M. Hernandez, J. Tejada, Phys. Rev. B **78**, 134501 (2008).
[12] R. Prozorov, A. F. Fidler,J. R. Hoberg, P.C. Canfield, Nature Physics **4**, 327 (2008).
[13] A. D. Hernandez, and D. Dominguez, Phys. Rev B **72**, 020505 (2005).
[14] J. R. Clem, R.P. Huebner, D. E. Gallus, Journal of Low Temperature Physics, **12**, 449 (1973)
[15] R. Prozorov, W. G. Russell, A. P. Anatolii, K. P. Garry, Phys. Rev. B **72**, 212508, (2005).
[16] R. Prozorov, Phys. Rev. Lett. **98**, 257001 (2007).
[17] S.V*é*lez, C. Panades-Guinart, G. Abril, A. Garcia-Santiago, J. M. Hernandez, J. Tejada, Phys. Rev. B **78**, 134501 (2008).
[18] W. Treimer, O. Ebrahimi, N. Karakas, S. O .Seidel, Nucl. Inst. and Meth. A **651**, pp. 53-56; (2011).
[19] W. Treimer, O. Ebrahimi, N. Karakas, R. Prozorov, Phys. Rev. B **85**, 184522 1-9 (2012).
[20] S Aull, O Ebrahimi, N Karakas, J Knobloch, O Kugeler, W Treimer, Journ. of Phys., Conf. Series **340**, 012001, p 1 - 7, (2012)
[21] W. Treimer, U. Feye-Treimer, J. Appl. Cryst. **44**, p 1157-1163. (2011)
[22] W. Treimer, O. Ebrahimi N. Karakas, Appl. Phys. Lett.**101**, 162603 (2012)